An Automated Computer-Vision "Bubble-Counting" Technique to Characterise CO$_2$ Dissolution into an Acetonitrile Flow Stream in a Teflon AF-2400 Tube-in-Tube Flow Device

Matthew O'Brien*[a] and Ruxandra Moraru[a]

[a] Dr M. O'Brien, R. Moraru.
The Lennard-Jones Laboratories, Keele University, Keele, Borough of Newcastle-under-Lyme, Staffordshire, England, United Kingdom of Great Britain and Northern Ireland, ST5 5BG.

Abstract

A Teflon AF-2400 based tube-in-tube device was used to generate flow streams of CO$_2$ in acetonitrile and a computer-vision based 'bubble counting' technique was used to estimate the amount of CO$_2$ that had passed into solution whilst in the tube-in-tube device by quantifying the amount of CO$_2$ that left solution (forming separate gas-phase segments) downstream of the back-pressure regulator. For both CO$_2$ pressures used, there appeared to be a minimum residence time below which no CO$_2$ was observed to leave solution. This was assumed to be due to residual CO$_2$ below (or close to) the saturation concentration at atmospheric pressure and, by taking this into account, we were able to fit curves corresponding to simple gradient-driven diffusion and which closely matched previously obtained colorimetric titration data for the same system. The estimated value for the residual concentration of CO$_2$ (0.37 M) is higher than, but in reasonable general correspondence with, saturation concentrations previously reported for CO$_2$ in acetonitrile (0.27 M).

Introduction

Flow chemistry has emerged in recent years as an interesting alternative to more familiar batch reaction paradigms.[1] It can, in some cases, offer potential benefits. For instance, as only a relatively small amount of material is generally being processed at any one time (reactions being scaled over time rather than over dimension), it can sometimes provide enhanced safety, particularly in situations where hazardous intermediates or extremes of pressure of temperature are involved.[2] With fixed and typically small reactor dimensions, surface-area-to-volume ratios are generally high and (importantly) constant. This leads to enhanced and dependable interfacial mass and energy transfer, thereby facilitating scale-invariant transformations.[3]

A key interface in a number of important chemical transformations is the gas-liquid interface, and a variety of approaches have been developed to enhance and control this in the context of flow chemical systems.[4] We have shown that flow reactors based on the semipermeable amorphous fluoropolymer Teflon AF-2400 can provide efficient and controllable gas-liquid mixing, particularly in the 'tube-in-tube' configuration.[5] Continuous flow membrane reactors of this type have now been used, both in our laboratories and in those of a number of other research groups, with a wide range of reactive gasses including ozone,[6] CO$_2$,[7] hydrogen,[8] carbon-monoxide,[9] syngas,[10] ethylene,[11, 8c, 10a] ammonia,[12] dimethylamine (in combination with carbon-monoxide),[13] oxygen,[14, 8c] diazomethane,[15] formaldehyde[16] and fluoroform.[17]

Jensen and co-workers have modelled the mass-transport in these reactors[18] and their operation seems to be characterised by relatively straightforward gradient-driven diffusion phenomena (consistent with Fick's law of diffusion).[19]

In terms of the measurement of gas concentration in solution, a number of approaches have been used. As an indirect technique, the quantity of gas leaving solution downstream of the back-pressure regulator ('out-gassing' after the solution has decompressed to ambient pressure) can be used to

estimate the level of dissolved gas. In addition to the use of a simple gas burette, we have shown that visual 'bubble counting' approaches can be used to quantify this.[8a] Other, more recent, related examples of 'bubble counting' approaches have also been described by Cherkasov, Rebrov and coworkers,[20a] by Gavriilidis and coworkers,[14i] and by Riley and coworkers.[20b] An interesting investigation of outgassing from flow streams in microfluidic devices, used to obtain phase diagrams from pressure-volume-temperature measurements is described by Mostowfi and coworkers.[21] For gas molecules with suitable chromophores, inline spectroscopic methods (e.g. IR) can be used.[9b] If the gas molecule has acidic or basic functionality, inline colorimetric titration has been shown to be an effective method.[12, 7b] Jensen, Zhang and co-workers have made good use of mass-flow controllers/meters to directly measure the flow rate of gas flowing across the AF-2400 membrane into solution.[22]

In this manuscript, we describe the use of a computer-vision based 'bubble-counting' method to measure the out-gassing of CO_2 from a stream of acetonitrile emerging from a Teflon AF-2400 tube-in-tube device.

Results and Discussion

The apparatus setup used in this work is outlined in Figure 1.
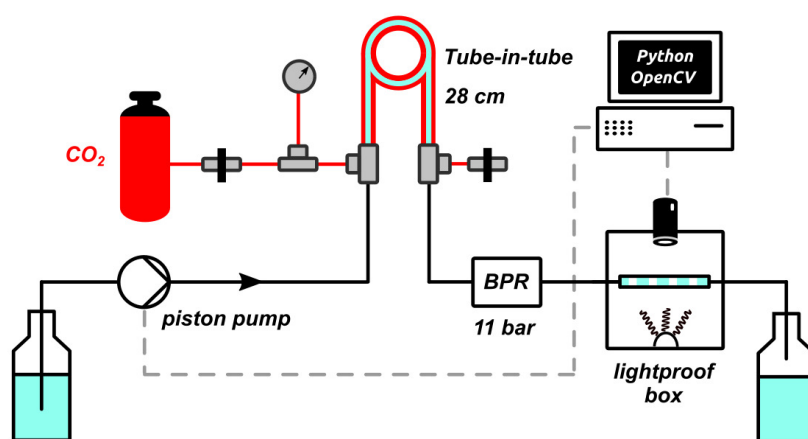
Figure 1. General apparatus setup.

A piston pump was used to pump the acetonitrile (which was used as purchased and not degassed) into the tube-in-tube device (28 cm of AF-2400, 6 mm ID held within an outer tube of PTFE, 1.59 mm ID). The outer tube was connected to the CO_2 cylinder via a poppet gas regulator. During operation, the outer tube was pressurised and the only exit for the CO_2 was to cross the membrane into solution. After passing through the tube-in-tube device, the solution passed through a 15 bar back-pressure regulator and then into a length of FEP tubing in an illuminated light-proof housing that was being continually monitored by a computer webcam. No gas segments were visible upstream of the back-pressure regulator (the flow stream was a homogeneous solution of gas in liquid). To facilitate the monitoring of the flow stream, a small quantity of lissamine green dye was added to the acetonitrile (40 mg L^{-1}). We assumed that the dye had no significant effect on the dissolution of CO_2. We also assumed that the amount of CO_2 still left in solution downstream of the back-pressure regulator would be significantly lower than the quantity of CO_2 in solution upstream of the back-pressure regulator (so that the amount of out-gassed CO_2 would be a reasonable lower estimate of the amount of CO_2 that entered the solution). The control and processing scripts were written in the Python[23] programming language. A simple graphic-user-interface was constructed

using the PyQt5[24] framework incorporating PyQtGraph[25] to monitor operation. Control of the piston pump was facilitated using PySerial.[26] Access to, and processing of, the video stream from the webcam was achieved using the OpenCV[27] computer-vision[28] library. Data processing, curve fitting and graph plotting were facilitated by Numpy,[29] Scipy[30] and Matplotlib.[31]

Using the colour of the lissamine green dye, the pixels in each frame of the video stream from the webcam were filtered according to their RGB value and pixels within a certain range were determined to be due to the dyed solvent.

Figure 2 A) A screenshot of an unprocessed frame from the webcam. B) Pixels filtered according to RGB value ('matching' pixels shown in white). A yellow bounding rectangle is shown around all clusters of matching pixels. A small number of 'noise' pixels can be seen on close inspection C) Image 'cleaned up' by performing opening/closing operations with an elliptical kernel to remove noise.

Shown in Figure 2 is an example of a frame from the webcam, alongside processed images. In Figure 2a, the blue-green dyed solution can be seen in the flow tubing. In Fig 2b, the pixels have been processed according to their RGB values and those within tolerance limits of matching the colour of the solvent are shown in white. Bounding rectangles have also been drawn around all clusters of matching pixels. A very small number of aberrant pixels/clusters can be seen. To remove such noise, the image was further processed by using opening/closing operations and the result is shown in Fig 2c, where there is only a single cluster of white pixels (within a single bounding rectangle).
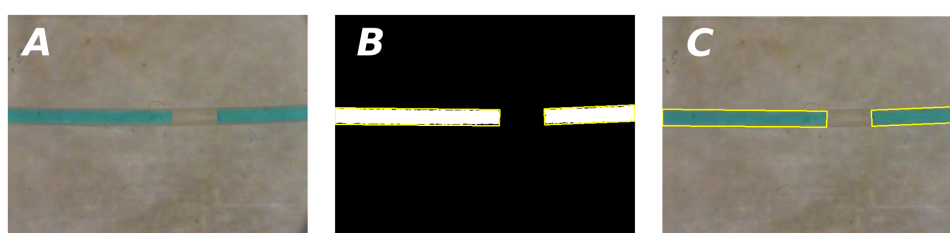
Figure 3. A) Unprocessed image from webcam that contains a gas 'bubble'. B) The processed image showing filtered pixels (in white) and the bounding rectangles in yellow. C) The original image with the bounding rectangles superimposed on it.

A sample of the processing when a gas bubble is present in the tubing is shown in Fig 3. The left-hand image shows the observed section of tubing with a gas segment present. The processed image is shown in Figure 3b and the two bounding rectangles for the segments of coloured pixels are superimposed on the original image in Figure 3c. As can be seen, the recognition of the pixels containing dye seems to be a reasonably faithful process. A certain amount of trial-and-error was required to find suitable lighting/brightness settings on the webcam (and tolerances on the filtration values) but, once these were found, they were used throughout.

To initiate a run, a button on the graphic user interface was pressed to obtain a calibration value (with the tubing filled with dye solution and with no gas bubbles present) and the tube-in-tube device would be pressurised to the required pressure. Another button on the graphic user interface would then be pressed to start the sequence of required flow rates on the piston pump. For each flow rate, a set of 900 frames were processed. Sufficient time at the beginning (and between each different flow rate) was also included so that the flow stream had completely flushed through the system. Data sets, one for each flow rate, were combined and saved in an .npy file along with the calibration value.

To analyse the data, we used the comparison of the total pixel count (of coloured pixels) with that of the total pixel count of the calibration image (obtained at the start of the process with no gas pressure/bubbles). The difference between the number of coloured pixels in each frame and the number of coloured pixels in the calibration image was taken to be proportional to the amount of gas that had left solution (as the gas segments contain no dyed solution). The number of coloured pixels was taken to be equally proportional to the volume of liquid. Division of the first number by the second number then gives the estimated concentration as a vol/vol ratio which can be converted to a mol/vol ratio using the density and molecular weight.

Shown in Figure 4 are the data sets for two different flow-rates/residence-times for a CO_2 pressure of 5 bar (gauge) at room temperature.
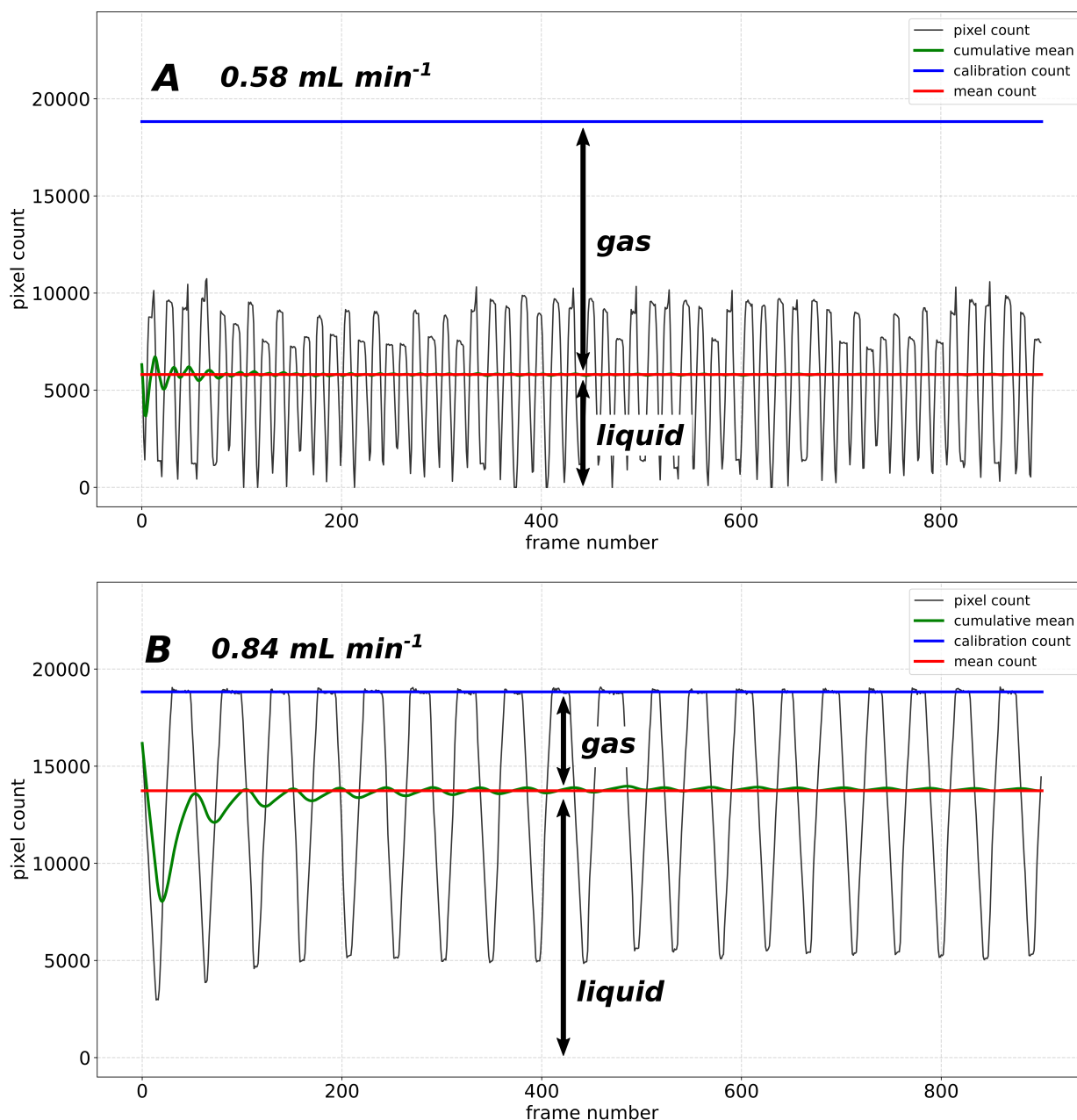
Figure 4. Pixel counts for 900 frames of video. A) Acetonitrile flow rate of 0.58 mL min^{-1} (residence time of 0.136 min). B) Acetonitrile flow rate of 0.84 mL min^{-1} (residence time of 0.094 min). Key: - pixel count, - cumulative mean, - calibration count, - mean count.

In Fig 4a, the acetonitrile flow rate was 0.58 mL min, which corresponds to a residence time of 0.136 min. As can be seen, the pattern of the pixel counts (of filtered pixels), which corresponds to the pattern of gas and liquid segments, has quite a periodic and regular nature. Occasionally, the pixel count touches zero, which corresponds to an image where the observed tubing is filled with gas. The calibration value (number of filtered pixels with no gas segments) is indicated with a blue horizontal line (18836 pixels). The average count of filtered pixels (5808) is shown as a red horizontal line. This represents the average volume of the liquid segments. The difference (13028) between this value and the calibration value represents the average volume of the gas segments. This gives a gas/liquid volume/volume ratio of 13028/5808 = 2.24 L (CO$_2$) L^{-1}. Using 1.842 g L^{-1} as the density of CO$_2$, this would lead to a concentration of 4.13 g L^{-1} or 0.094 mol L^{-1}. In Fig 4b, for a flow rate of 0.84 mL min (which now corresponds to a lower residence time of 0.094 min), there is

clearly a much higher level of filtered pixels (there is now more liquid than gas present in the tubing). The average count is 13736 and this would lead to a lower concentration of 0.371 L (CO_2) L^{-1} or 0.016 mol L^{-1}.

Also indicated in Fig 4 (in green) is the cumulative mean of the pixel count. In Fig 4b this is more easily noticed as it takes a significant number of frames (ca. 300) for this to match closely the actual mean over the 900 frames. This is due to the periodicity of the data (or rather the length of the period). When the pixel count is at the same level as the calibration value (where it hits the blue 'calibration' line), this represents frames where there are no gas segments in the image at all. The 'dips' in the data curve represent single (but relatively large) segments of gas passing across the video image. In Fig 4a, although there is a greater quantity of total gas segment present, the segments are much smaller and this leads to a much lower period length for the data pattern, hence the rapidity with which the cumulative mean converges to the actual mean.

Using the same approach across a range of flow-rates/residence-times, a plot of out-gassed CO_2 (per unit volume of solvent) against residence-time (for data obtained at both 5 and 10 bar of CO_2 pressure) is shown in Fig 5.
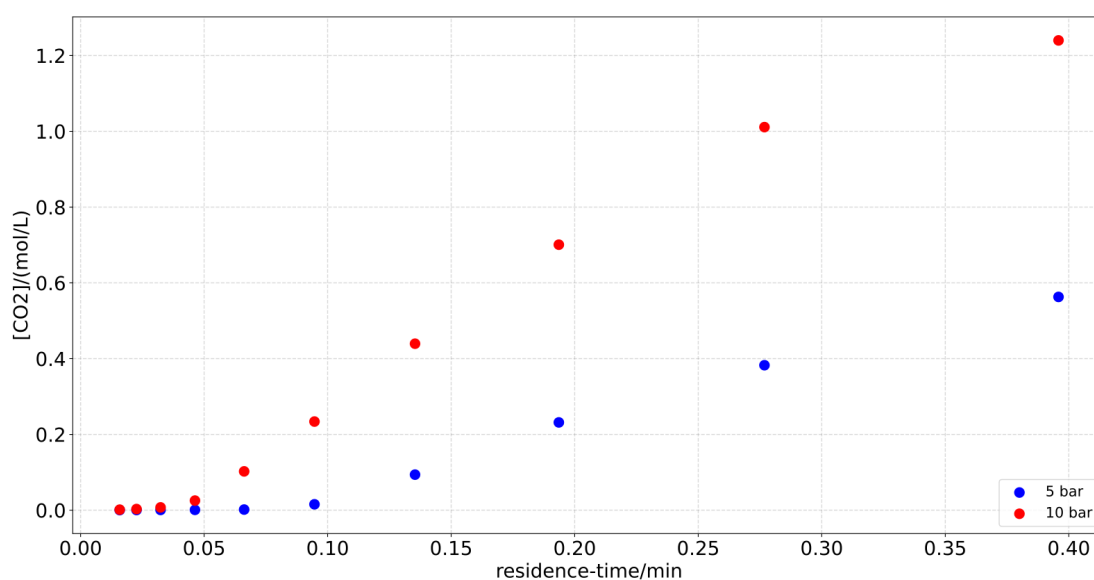
Figure 5. Data for out-gassed CO_2 per unit volume of acetonitrile (in mol L^{-1}) against residence time of the liquid in the tube-in-tube device. Key: • 5 bar, • 10 bar.

As might be expected, the level of out-gassed CO_2 increases with increasing residence time, and the slope of the curve at higher residence times also seems to diminish with increasing residence time, in line with simple gradient driven diffusion (i.e. indicating that the curve may eventually plateau at the saturation concentration at high enough residence time). However, it is noteworthy that, for both curves, there seems to be an apparent 'induction' period close to zero residence time. There seems to be a lower limit of residence time for each curve below which there is no observed out-gassing downstream of the back-pressure regulator. As we would generally expect there to be some non-zero CO_2 concentration for all non-zero residence times, the observed out-gassing does not appear to correlate directly with CO_2 concentration.

If we compare these data with those previously obtained in our previous study of the same CO_2/acetonitrile/AF-2400 system using an inline colorimetric titration, the difference can clearly be seen (Figure 6).
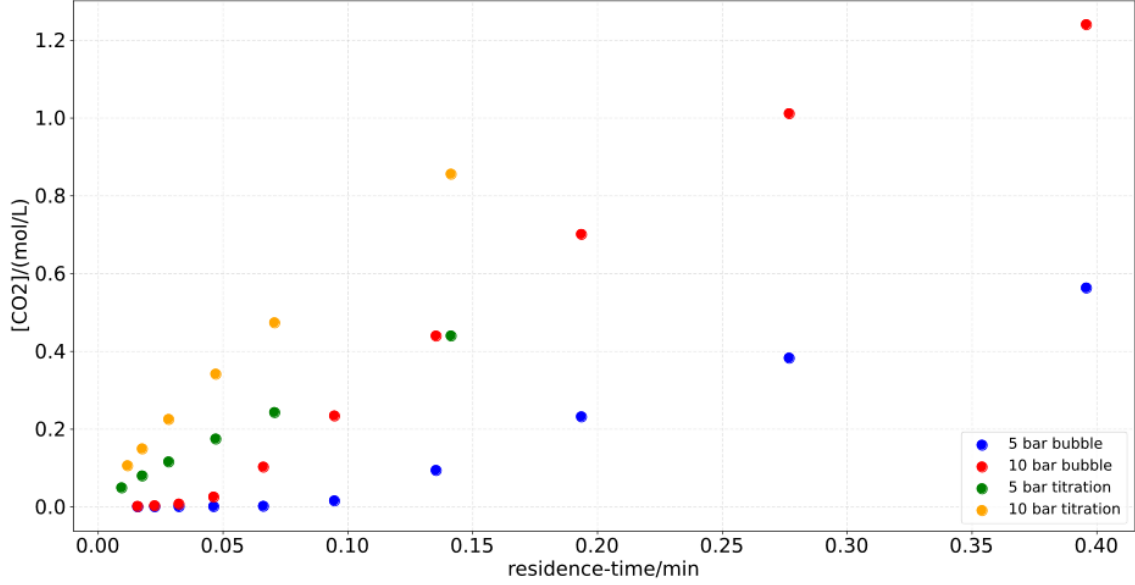
Figure 6. Data for out-gassed CO_2 alongside previously obtained concentration values using colorimetric inline titration. Key: • 5 bar 'bubble counting', • 10 bar 'bubble counting',: • 5 bar titration, • 10 bar titration.

An explanation for this difference lies in the fact that some residual CO_2 may remain in solution even after the solution has exited the back-pressure regulator (where it can decompress to atmospheric pressure). If the concentration of CO_2 is below its saturation concentration at atmospheric pressure, it should remain in solution rather than forming gas segments. Only when the acetonitrile has had sufficient time in the tube-in-tube device to reach a CO_2 concentration higher than this level will CO_2 likely be observed to outgas (as the solution will be super-saturated once it passes through the back-pressure regulator). The amount of CO_2 in the gas segments would then be equal to the total quantity of CO_2 taken up whilst in the tube-in-tube device minus this residual amount of CO_2 that remains in solution (or zero, whichever is highest – as it is obviously impossible to have a negative volume of gas phase). The colorimetric titration, on the other hand, will be sensitive to all dissolved CO_2 in solution and, as such, will indicate a positive titre for all residence times, only giving a zero value for zero residence time.

If the residual CO_2, **R**, after out-gassing is taken into account as in the following:

$$[\mathbf{CO_2}]^{(obs)} = \mathbf{max}([\mathbf{CO_2}] - \mathbf{R}, \mathbf{0}) \qquad (1)$$

(where $[\mathbf{CO_2}]^{(obs)}$ is the observed out-gassing CO_2) and the actual concentration of CO_2 is given by the usual gradient driven diffusion equation (**2**):

$$[\mathbf{CO_2}] = S(1 - e^{-kt}) \qquad\qquad\qquad (2)$$

(where S is the saturation concentration, k is a kinetic parameter for the rate of diffusion and t is time) we have:

$$[\mathbf{CO_2}]^{(obs)} = \boldsymbol{max}\big(S(1 - e^{-kt}) - R, 0\big) \qquad\qquad (3)$$

We used the least squares (leastsq) module of SciPy to fit the S, k and R parameters in (3) to the observed out-gassing data, with individual S and k values for each of the 5 and 10 bar data sets but with a common value of R for both data sets (as the solution decompresses to the same atmospheric pressure downstream of the back-pressure regulator regardless of the CO_2 pressure in the tube-in-tube device – so we might expect the residual remaining CO_2 to have the same value). This gave the following curves:
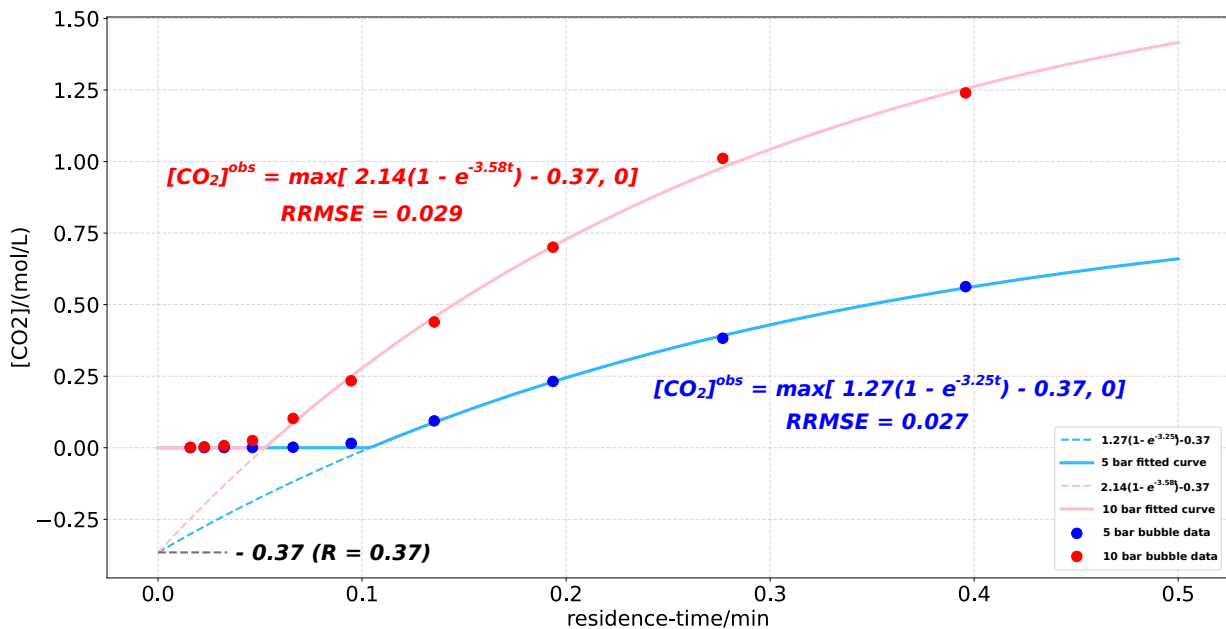
Figure 7. Fitted curves for the observed bubble counting data for 5 and 10 bar pressures. RRMSE = Relative Root Mean Square Error. Key: • 5 bar 'bubble counting', • 10 bar 'bubble counting', - fitted curve for 5 bar data, - Fitted curve for 10 bar data, - - 'extension' of fitted 5 bar curve below horizontal axis, - - 'extension' of fitted curve for 10 bar data below horizontal axis.

The two curves are shown in solid blue and red lines and the 'extensions' of the curves beyond the horizontal axis are shown with dashed lines (which naturally both intercept the vertical axis at the same value of -0.37, corresponding with the presumed common estimated residual CO_2 value R). If the fitted values for S and k for these curves are then used in the standard $[\mathbf{CO_2}] = S(1 - e^{-kt})$ equation, this gives the following graph:
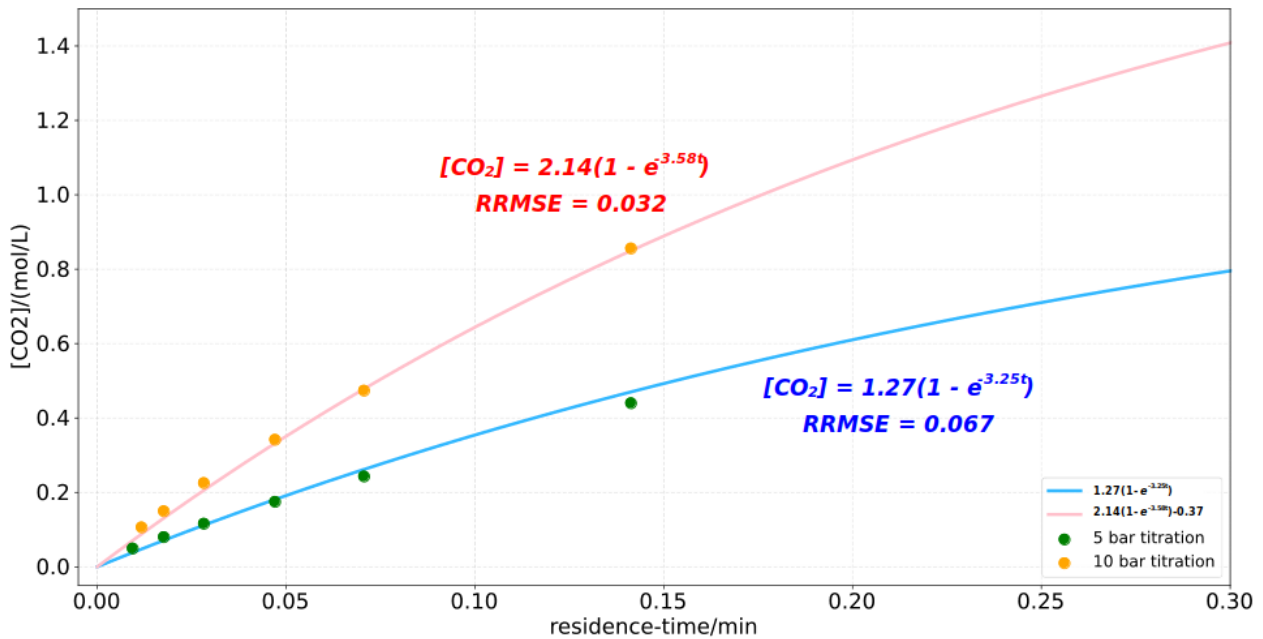
Figure 8. Using the *S* and *k* values fitted from the bubble counting data to plot $[CO_2] = S(1 - e^{-kt})$ and comparison with titration data. RRMSE = Relative Root Mean Square Error. Key: • 5 bar data points form inline titration. • 10 bar data points form inline titration. — $S(1 - e^{-kt})$ curve using *S* and *k* parameters from 5 bar bubble-counting data. — $S(1 - e^{-kt})$ curve using *S* and *k* parameters from 10 bar bubble-counting data.

As can be seen, there is reasonably good agreement between the fitted curves and the experimental titration data. A comparison of these curves with the previously fitted curves for the titration data is shown in Figure 9.
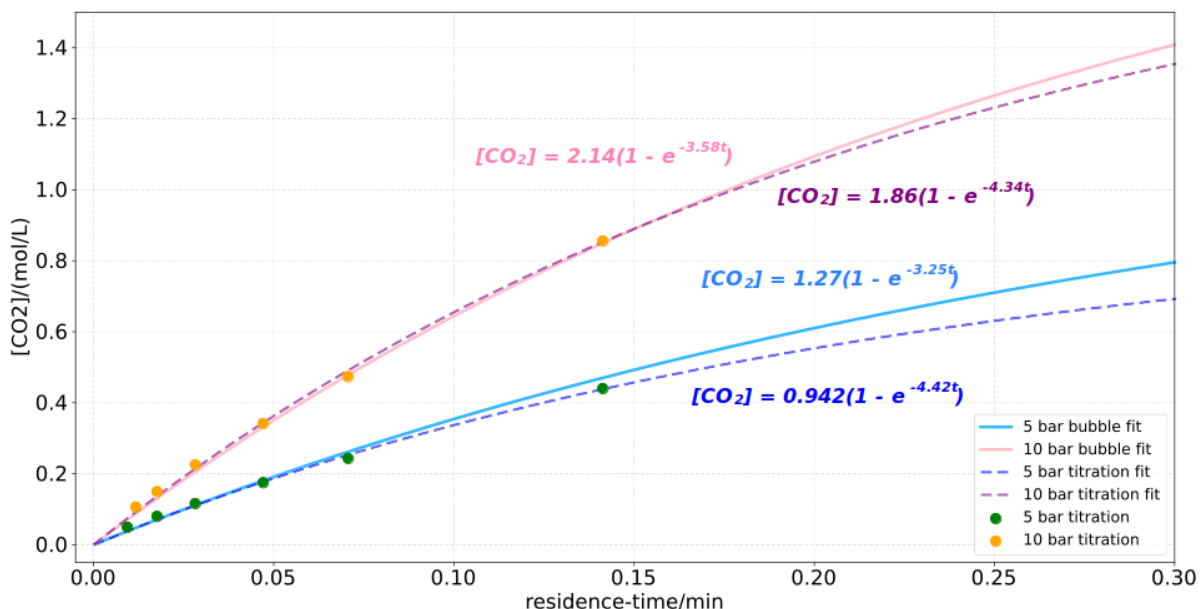
Figure 9. Comparison of curves fitted to the bubble counting data (with the residual CO_2, *R*, removed) with curves previously fitted to the titration data. Key: • 5 bar data points from inline titration. • 10 bar data points from inline titration. — fitted 5 bar $S(1 - e^{-kt})$. — fitted 10 bar $S(1 - e^{-kt})$. - - previously fitted 5 bar curve from titration data. - - previously fitted 10 bar curve from titration data.

Although there is some difference between the **S** and **k** parameters, there is reasonable overall agreement between the two. Clearly, to obtain greater precision for these parameters (either using a non-linear curve fitting or following linearisation) a larger number of data points would be required, probably including some closer to the saturation point to get a more meaningful estimate of **S**. Regarding the estimated value (0.37 M) of **R**, which is an estimate of the residual quantity of CO_2 that does not out-gas, this might be expected to provide a reasonable estimate of the saturation solubility of CO_2 at atmospheric pressure. Whilst it is higher than the value of 0.27 M reported[32] for the solubility of CO_2 in acetonitrile, it is not unreasonably dissimilar. One explanation (other than experimental error etc) for the higher value could be that the solvent segments remain temporarily supersaturated to a certain degree. A greater amount of time might be required for all of the CO_2 (above the saturation concentration) to fully leave solution. This might be achieved by using a longer length of tubing between the back-pressure regulator and the webcam stage, and the dependence of the relative size of the gas and liquid segments on time could also be investigated by 'storing' (and subsequently monitoring) a static section of output stream. Due to some resistance to flow in this section of tubing, it is also possible that the pressure of the liquid remains somewhat above atmospheric and this could impart some effect.[33] Addtionally, as the 'useful' data points (with non-zero outgassing) are, by definition, not very close to the intercept with the vertical axis, the value of **R** in the curve fitting process might be fairly susceptible to noise and errors.

Conclusion

We have described the development of a computer-vision based 'bubble counting' approach to quantify the observed out-gassing of CO_2 from a flowing acetonitrile solution generated using a Teflon AF-2400 tube-in-tube device. Although the dependence of the quantity of out-gassed CO_2 on residence time is similar to the dependence on residence time of CO_2 concentrations as previously measured by inline colorimetric titration, there appears to be an 'induction' residence time below which no CO_2 is observed to out-gas from the generated flow stream. This might be ascribed to the residual CO_2 which (if below the saturation concentration at atmospheric pressure) should remain in solution. By taking this into account, we have shown that the measurement of out-gassing can still be approximated by a simple gradient-driven diffusion model and can lead to fitted curves that closely match the inline titration data. We are currently working on the collection and analysis of larger data sets to further investigate the validity of the approach, and whether any refinements or modifications are needed, and will report our findings in due course.

Experimental

Acetonitrile (analytical HPLC grade) was purchased from Fisher Scientific and used without further purification. Carbon dioxide was supplied by BOC gases and a GasArc Techmaster single stage regulator was used to regulate the pressure. The HPLC pump used was a Knauer Azura P 4.1 S. A USB-to-RS232 interface (Newlink USB-0039DBL USB-to-RS232 adapter, purchased from CPC/Farnell) was used to connect this (using a crossover-serial/null-modem cable) to the control computer. The webcam used was a Microsoft Lifecam Cinema. Aside from the Tube-in-Tube device, FEP or PFA flow tubing was used (1.0 mm o.d 0.6 mm i.d.) and connected using Omnifit/Diba adapters and interconnects (1/4-28-UNF thread). The back-pressure regulator was an Upchurch/IDEX type (Kinesis UK) and was manually adjusted to provide the desired back pressure of 11 bar (gauge), as measured using the pressure meter of the Knauer Azura pump. A diffused USB-powered LED light (XY-store, Amazon UK) was used to illuminate the flow stream at the webcam, and was powered by a separate USB-type power supply. Gas valves, and t-peice interconnects on the tube-in-tube device were supplied by Swagelok UK. The work was carried out at room temperature (20 °C).

References

1) Selected articles and reviews: a) S. V. Ley, *Chmical Record* **2012**, 12/4, 378-390. b) J. I. Yoshida, *Chemical Record* **2010**, 10/5, 332-341. c) J. A. M. Lummiss, P. D. Morse, R. L. Beingessner, T. F. Jamison, *Chemical Record* **2017**, 17/7, 667-680. d) D. T. McQuade, P. H. Seeberger, *J. Org. Chem.* **2013**, 78/13, 6384-6389. e) M. Movsisyan, E. I. P. Delbeke, J. Berton, C. Battilocchio, S. V. Ley, C. V. Stevens, *Chem. Soc. Rev.* **2016**, 45/18, 4892-4928. f) J. C. Pastre, D. L. Browne, S. V. Ley, *Chem. Soc. Rev.* **2013**, 42/23, 8849-8869. g) H. P. L. Gemoets, Y. H. Su, M. J. Shang, V. Hessel, R. Luque, T. Noel, *Chem. Soc. Rev.* **2016**, 45/1, 83-117. h) V. Hessel, D. Kralisch, N. Kockmann, T. Noel, Q. Wang, *ChemSusChem* **2013**, 6/5, 746-789. i) H. Amii, A. Nagaki, J. Yoshida, *Beilstein J. Org. Chem.* **2013**, 9, 2793-2802. j) J. Wegner, S. Ceylan, A. Kirschning, *Adv. Synth. Catal.* **2012**, 354/1, 17-57. k) T. Fukuyama, T. Totoki, I. Ryu, *Green Chem.* **2014**, 16/4, 2042-2050. l) S. T. R. Müller, T. Wirth, *ChemSusChem* **2015**, 8/2, 245-250. m) S. G. Newman, K. F. Jensen, *Green Chem.* **2013**, 15/6, 1456-1472. n) D. Webb, T. F. Jamison, *Chem. Sci.* **2010**, 1/6, 675-680. o) C. Wiles, P. Watts, *Chem. Commun.* **2011**, 47/23, 6512-6535. p) M. Baumann, I. R. Baxendale, *Beilstein J. Org. Chem.* **2015**, 11, 1194-1219. q) B. Gutmann, D. Cantillo, C. O. Kappe, *Angew. Chem. Int. Ed.* **2015**, 54/23, 6688-6728.

2) a) A. Bonner, A. Loftus, A. C. Padgham, M. Baumann, *Org. Biomol. Chem.* **2021**, 19/36, 7737-7753. b) M. Vaz, D. Courboin, M. Winter, P. M. C. Roth. *Org. Proc. Res. Dev.* **2021**, 25/7, 1589-1597.

3) a) R. L. Hartman, J. P. McMullen, K. F. Jensen, *Angew. Chem. Int. Ed.*, **2011**, 50/33, 7502-7519. b) J. P. Knowles, L. D. Elliott, K. I. Booker-Milburn, *Beilstein J. Org. Chem.* **2012**, 8, 2025-2052.

4) Selected articles and reviews: a) J. Kobayashi, Y. Mori, K. Okamoto, R. Akiyama, M. Ueno, T. Kitamori, S. Kobayashi, *Science* **2004**, 304/5675, 1305-1308. b) R. D. Chambers, M. A. Fox, G. Sandford, *Lab Chip* **2005**, 5/10, 1132-1139. c) Y. Wada, M. M. Schmidt, K. F. Jensen, *Ind. Eng. Chem. Res.* **2006**, 45/24, 8036-8042. d) K. Jähnisch, M. Baerns, V. Hessel, W. Ehrfeld, V. Haverkamp, H. Löwe, C. Wille, A. Guber, *J. Fluorine Chem.* **2000**, 105/1, 117-128. e) M. T. Rahman, T. Fukuyama, N. Kamata, M. Sato, I. Ryu, *Chem. Commun.* **2006**, 21, 2236-2238. f) N. Yoswathananont, K. Nitta, Y. Nishiuchi, M. Sato, *Chem. Commun.* **2005**, 1, 40-42. g) B. Desai, C. O. Kappe, *J. Comb. Chem.* **2005**, 7/5, 641-643. h) I. R. Baxendale, J. Deeley, C. M. Griffiths-Jones, S. V. Ley, S. Saaby, G. K. Tranmer, *Chem. Commun.* **2006**, 24, 2566-2568. i) M. O'Brien, A. Polyzos, A. in *Flow Chemistry in Organic Synthesis*, **2018**, editors: T. F. Jamison, G. Koch, Book Series: *Science of Synthesis*; p. 243-272. Published by Georg Thieme Verlag AG.

5) M. Brzozowski, M. O'Brien, S. V. Ley, A. Polyzos, *Acc. Chem. Res.* **2015**, 48/2, 349-362.

6)   a) M. O'Brien, I. R. Baxendale, S. V. Ley, *Org. Lett.* **2010**, 12/7, 1596-1598. b) C. X. Sun, Y. Y. Zhao, J. M. Curtis, *Anal. Chim. Acta* **2013**, 762, 68-75.

7)   a) A. Polyzos, M. O'Brien, T. P. Petersen, I. R. Baxendale, S. V. Ley, *Angew. Chem. Int. Ed.* **2011**, 50/5, 1190-1193. b) M. O'Brien, *J. CO_2 Util.* **2017**, 21, 580-588. c) J. J. F. van Gool, S. van den Broek, R. M. Ripken, P. J. Nieuwland, K. Koch, F. Rutjes, *Chem. Eng. Technol.* **2013**, 36/6, 1042-1046. d) A. Rehman, A. M. L. Fernandez, M. Resul, A. Harvey, *J. CO_2 Util.* **2018**, 24, 341-349. e) J. A. Newby, D. W. Blaylock, P. M. Witt, J. C. Pastre, M. K. Zacharova, S. V. Ley, D. L. Browne, *Org. Proc. Res. Dev.* **2014**, 18/10, 1211-1220.

8)   a) M. O'Brien, N. Taylor, A. Polyzos, I. R. Baxendale, S. V. Ley, *Chem. Sci.* **2011**, 2/7, 1250-1257. b) S. Newton, S. V. Ley, E. C. Arcé, D. M. Grainger, *Adv. Synth. Catal.* **2012**, 354/9, 1805-1812. c) S.-H. Lau, S. L. Bourne, B. Martin, B. Schenkel, G. Penn, S. V. Ley, *Org. Lett.* **2015**, 17/21, 5436-5439. d) B. Venezia, L. Panariello, D. Biri, J. Shin, S. Damilos, A. N. P. Radhakrishnan, C. Blackman, A. Gavriilidis, *Catalysis Today*, **2021**, 362, 104-112. e) Y. M. Mo, J. Imbrogno, H. M. Zhang, K. F. Jensen, *Green Chem.* **2018**, 20, 3867-3874.

9)   a) P. Koos, U. Gross, A. Polyzos, M. O'Brien, I. R. Baxendale, S. V. Ley, *Org. Biomol. Chem.* **2011**, 9/20, 6903-6908. b) S. V. F. Hansen, Z. E. Wilson, T. Ulven, S. V. Ley, *React. Chem. Eng.* **2016**, 1/3, 280-287. c) C. Brancour, T. Fukuyama, Y. Mukai, T. Skrydstrup, I. Ryu, *Org. Lett.* **2013**, 15/11, 2794-2797.

10) a) S. L. Bourne, M. O'Brien, S. Kasinathan, P. Koos, P. Tolstoy, D. X. Hu, R. W. Bates, B. Martin, B. Schenkel, S. V. Ley, *ChemCatChem* **2013**, 5/1, 159-172. b) S. Kasinathan, S. L. Bourne, P. Tolstoy, P. Koos, M. O'Brien, R. W. Bates, I. R. Baxendale, S. V. Ley, *SynLett* **2011**, 18, 2648-2651.

11) a) C. Battilocchio, G. Iannucci, S. Wang, E. Godineau, A. Kolleth, A. De Mesmaeker, S. V. Ley, *React. Chem. Eng.* **2017**, 2/3, 295-298. b) C. Schotten, D. Plaza, S. Manzini, S. P. Nolan, S. V. Ley, D. L. Browne, A. Lapkin, *ACS Sustainable Chem. Eng.* **2015**, 3/7, 1453-1459. c) S. L. Bourne, P. Koos, M. O'Brien, B. Martin, B. Schenkel, I. R. Baxendale, S. V. Ley, *SynLett* **2011**, 18, 2643-2647. d) J. Morvan, T. McBride, I. Curbet, S. Colombel-Rouen, T. Roisnel, C. Crévisy, D. L. Browne, M. Mauduit, *Angew. Chem. Int. Ed.* **2021**, 60, 19685-19690.

12) a) J. C. Pastre, D. L. Browne, M. O'Brien, S. V. Ley, *Org. Proc. Res. Dev.* **2013**, 17/9, 1183-1191. b) D. L. Browne, M. O'Brien, P. Koos, P. B. Cranwell, A. Polyzos, S. V. Ley, *SynLett* **2012**, 23/9, 1402-1406. c) P. B. Cranwell, M. O'Brien, D. L. Browne, P. Koos, A. Polyzos, M. Peña-López, S. V. Ley, *Org. Biomol. Chem.* **2012**, 10/30, 5774-5779.

13) U. Gross, P. Koos, M. O'Brien, A. Polyzos, S. V. Ley, *Eur. J. Org. Chem.* **2014**, 29, 6418-6430.

14) a) S. R. Chaudhuri, J. Hartwig, L. Kupracz, T. Kodanek, J. Wegner, A. Kirschning, A., *Adv. Synth. Catal.* **2014**, 356/17, 3530-3538. b) T. P. Petersen, A. Polyzos, M. O'Brien, T. Ulven, I. R. Baxendale, S. V. Ley, *ChemSusChem* **2012**, 5/2, 274-277. c) B. Tomaszewski, R. C. Lloyd, A. J. Warr, K. Buehler, A. Schmid, A., *ChemCatChem* **2014**, 6/9, 2567-2576. d) B. Tomaszewski, A. Schmid, K. Buehler, *Org. Proc. Res. Dev.* **2014**, 18/11, 1516-1526. e) M. Brzozowski, J. A. Forni, G. P. Savage, A. Polyzos, *Chem. Commun.* **2015**, 51/2, 334-337. f) S. Sharma, R. A. Maurya, K. I. Min, G. Y. Jeong, D. P. Kim, *Angew. Chem. Int. Ed.* **2013**, 52/29, 7564-7568. g) J. H. Park, C. Y. Park, M. J. Kim, M. U. Kim, Y. J. Kim, G. H. Kim, C. P. Park, *Org. Proc. Res. Dev.* **2015**, 19/7, 812-818. h) B. Venezia, M. Douthwaite, G. W. Wu, M.

Sankar, P. Ellis, G. J. Hutchings, A. Gavriilidis, *Chem. Eng. J.* **2019**, 378, #122250. i) G. W. Wu, E. H. Cao, S. Kuhn, A. Gavriilidis, *Chem. Eng. Technol.*, **2017**, 40/12, 2346-2350.

15) a) D. Dallinger, C. O. Kappe, *Nature Protocols* **2017**, 12/10, 2138-2147. b) D. Dallinger, V. D. Pinho, B. Gutmann, C. O. Kappe, *J. Org. Chem.* **2016**, 81/14, 5814-5823. c) S. Garbarino, J. Guerra, P. Poechlauer, B. Gutmann, C. O. Kappe, *J. Flow Chem.* **2016**, 6/3, 211-217. d) H. F. Koolman, S. Kantor, A. R. Bogdan, Y. Wang, J. Y. Pan, S. W. Djuric, *Org. Biomol. Chem.* **2016**, 14/27, 6591-6595. e) V. D. Pinho, B. Gutmann, L. S. M. Miranda, R. de Souza, C. O. Kappe, *J. Org. Chem.* **2014**, 79/4, 1555-1562. f) F. Mastronardi, B. Gutmann, C. O. Kappe, *Org. Lett.* **2013**, 15/21, 5590-5593.

16) A. E. Buba, S. Koch, H. Kunz, H. Löwe, *Eur. J. Org. Chem.* **2013**, 21, 4509-4513.

17) B. Musio, E. Gala, S. V. Ley, *ACS Sustainable Chem. Eng.* **2018**, 6/1, 1489-1495.

18) L. Yang, K. F. Jensen, *Org. Proc. Res. Dev.* **2013**, 17/6, 927-933.

19) a) A. Fick, *Annalen der Physik*, **1855**, 170/1, 59–86. b) A. Fick, *Phil. Mag.* **1855**, 10/63, 30–39.

20) a) N. Cherkasov, A. J. Expósito, B. Y. Bai, E. V. Rebrov, *React. Chem. Eng.*, **2019**, 4, 112-121. b) N. C. Neyt, C. J. van der Westhuizen, J. L. Panayides, D. L. Riley, *React. Chem. Eng.* **2022**; accepted-article; https://doi.org/10.1039/D1RE00554E.

21) F. Mostowfi, S. Molla, P. Tabeling., *Lab Chip*, **2012**, 12, 4381-4387.

22) a) J. S. Zhang, A. Teixeira, H. M. Zhang, K. F. Jensen, *React. Chem. Eng.* **2020**, 5/1, 51-57. b) X. N. Duan, J. C. Tu, A. R. Teixeira, L. Sang, K. F. Jensen, J. S. Zhang, *React. Chem. Eng.* **2020**, 5/9, 1751-1758. c) C. J. Zhou, B. Q. Xie, S. W. Li, J. S. Zhang, *AIChe Journal*, **2020**, 66/11, #e17015.

23) a) http://www.python.org (accessed 1st May 2022). b) Centrum voor Wiskunde en Informatica 1995. Python tutorial. *Technical Report CS-R9526*. Amsterdam: van Rossum, G.

24) https://riverbankcomputing.com/software/pyqt/ (accessed 1st May 2022).

25) https://www.pyqtgraph.org/ (accessed 1st May 2022).

26) https://github.com/pyserial/pyserial/ (accessed 1st May 2022).

27) a) G. Bradski, *Dr. Dobbs J.*, **2000**, 25, 120-125. b) https://opencv.org/ (accessed 1st May 2022).

28) For some further related examples of the use of computer-vision in chemistry applications see: a) M. O'Brien, A. Hall, J. Schrauwen, J. van der Made, J.; *Tetrahedron*, **2018**, 74/25, 3152-3157. b) M. O'Brien, L. Konings, M. Martin, J. Heap, *Tetrahedron Lett.* **2017**, 58, 2409-2413. c) M. O'Brien, D. A. Cooper, J. Dolan, J. *Tetrahedron Lett.* **2017**, 58, 829-834. d) M. O'Brien, D. Cooper, *Synlett* **2016**, 27, 164-168. e) M. O'Brien, D. A. Cooper, P. Mhembere, *Tetrahedron Lett.* **2016**, 57, 5188-5191. f) M. O'Brien, P. Koos, D. L. Browne, S. V. Ley, *Org. Biomol. Chem.* **2012**, 10, 7031-7036. g) S. V. Ley, R. J. Ingham, M. O'Brien, D. L. Browne, *Beilstein J. Org. Chem.* **2013**, 9, 1051-1072.

29) a) C. R. Harris, K. J. Millman, S. J. van der Walt, R. Gommers, P. Virtanen, D. Cournapeau, E. Wieser, J. Taylor, S. Berg, N. J. Smith, R. Kern, M. Picus, S. Hoyer, M. H. van Kerkwijk, M. Brett, A. Haldane, J. Fernández del Río, M. Wiebe, P. Peterson, P. Gérard-Marchant, K. Sheppard, T. Reddy, W. Weckesser, H. Abbasi, C. Gohlke, T. E. Oliphant *Nature* **2020**, 585, 357–362. DOI: 10.1038/s41586-020-2649-2. b) https://numpy.org (accessed 1st May 2022).

30) a) https://scipy.org (accessed 1st May 2022) b) P. Virtanen, R. Gommers, T. E. Oliphant, M. Haberland, T. Reddy, D. Cournapeau, E. Burovski, P. Peterson, W. Weckesser, J. Bright, S. J. van der Walt, M. Brett, J. Wilson, K. J. Millman, N. Mayorov, A. R. J. Nelson, E. Jones, R. Kern, E. Larson, C. J. Carey, I. Polat, Y. Feng, E. W. Moore, J. VanderPlas, D. Laxalde, J. Perktold, R. Cimrman, I. Henriksen, E. A. Quintero, C. R. Harris, A. M. Archibald, A. H. Ribeiro, F. Pedregosa, P. van Mulbregt, and SciPy 1.0 Contributors. *Nature Methods* **2020**, 17/3, 261-272. b) https://scipy.org (accessed 1st May 2022).

31) a) https://matplotlib.org (accessed 1st May 2022) b) J. D. Hunter, *Computing in Sci. & Eng.* **2007**, 9/3, 90-95.

32) Y. Tomita, S. Teruya, O. Koga, Y. Hori, *J. Electrochem. Soc.* **2000**, 147/11, 4164-4167.

33) For articles relevant to the process/mechanism of outgassing in flow streams, see: ref [21], also: a) B. Bao, J. Riordon, F. Mostowfi, D. Sinton., *Lab Chip,* **2017**, 17, 2740-2759. b) M. Blander, J. L. Katz, *AIChe Journal*, **1975**, 21/5, 833-848. c) R. M. Ripken, J. A. Wood, S. Schlautmann, A. Günther, H. J. G. E. Gardeniers, S. Le Gac, *React. Chem. Eng.* **2021**, 6, 1869-1877. d) K. J. Vachaparimbil, K. E. Einarsrud, *J. Electrochem. Soc.*, **2018**, 165/10, E504-E512.

Table of Contents Graphic:

MeCN → Tube-in-Tube → CO$_2$ in MeCN

CO$_2$ · Tube-in-tube 28 cm · Python OpenCV · piston pump · BPR 11 bar · lightproof box
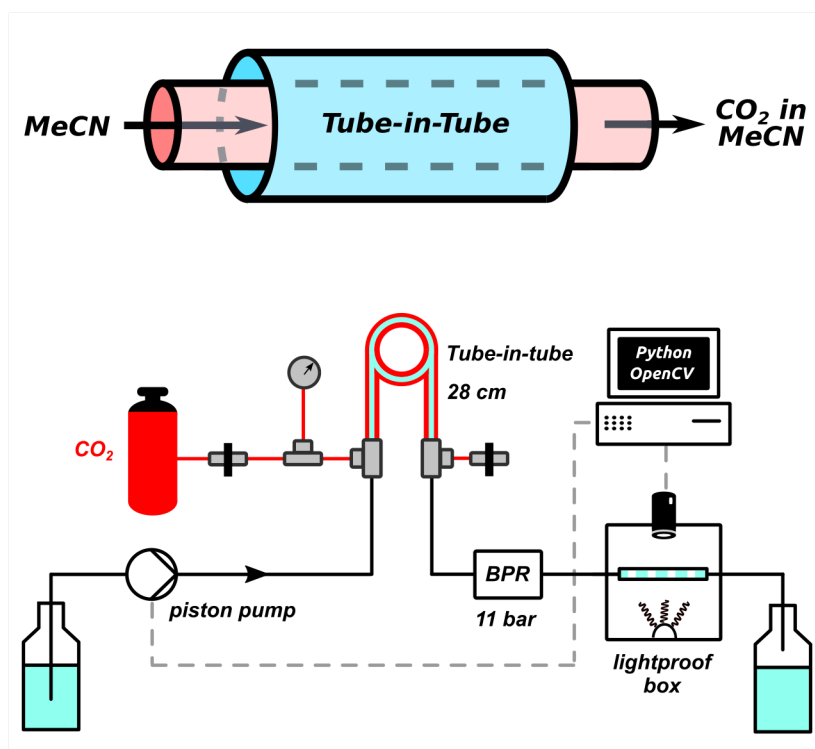
A computer-vision 'bubble counting' approach was used to estimate CO_2 dissolution into acetonitrile in a Teflon AF-2400 tube-in-tube device. The observed differences to our previously reported methodology (inline titration) can be accounted for if residual dissolved CO_2 (that doesn't outgas) is taken into consideration.